

One-loop squared amplitudes for hadronic tW production at next-to-next-to-leading order in QCD

Long-Bin Chen,^a Liang Dong,^b Hai Tao Li,^{b,1} Zhao Li,^{c,d,e} Jian Wang,^{b,2} and Yefan Wang^b

^a*School of physics and materials science, Guangzhou University, Guangzhou 510006, China*

^b*School of Physics, Shandong University, Jinan, Shandong 250100, China*

^c*Institute of High Energy Physics, Chinese Academy of Sciences, Beijing 100049, China*

^d*School of Physics Sciences, University of Chinese Academy of Sciences, Beijing 100039, China*

^e*Center of High Energy Physics, Peking University, Beijing 100871, China*

E-mail: chenlb@gzhu.edu.cn, liang.dong@mail.sdu.edu.cn,
haitao.li@sdu.edu.cn, zhaoli@ihep.ac.cn, j.wang@sdu.edu.cn,
wangyefan@sdu.edu.cn

ABSTRACT: We present the analytic results of one-loop squared amplitudes for tW production at a hadron collider. The calculation is performed using the method of differential equations. After renormalization, we have checked that the infrared divergences agree with the general structure predicted by anomalous dimensions. The finite remainder contributes to the next-to-next-to-leading order hard function, one of the essential ingredients in the factorization formula of the cross section near the infrared region, which can be used in resummation of all-order soft gluon effects or a differential next-to-next-to-leading order calculation based on the phase space slicing method.

¹Corresponding author.

²Corresponding author.

Contents

1	Introduction	1
2	Kinematics and notations	3
3	One-loop calculation	4
3.1	Bare loop amplitudes	4
3.2	Renormalization	8
3.3	Infrared divergences	9
4	Expansion in m_W^2	13
5	Conclusions	16
A	Rational matrices and boundary conditions for the second integral family	17
B	Perturbative expansion of renormalization factors	18

1 Introduction

The top quark is the heaviest elementary particle in the Standard Model (SM) and may play an essential role in the electroweak symmetry breaking due to its large coupling with the Higgs boson. Its short lifetime also allows the study on its various properties as a “bare” quark without hadronization. Meanwhile the W boson couples with many SM particles via gauge interactions and therefore could be sensitive to the new physics beyond the SM with such interactions modified. The recent precise measurement of the CDF collaboration on the W boson mass [1] has shed light on a significant tension with the other experimental observations in the assumption of the SM electroweak framework. Especially the strong correlation between the top quark and the W boson implies that the precise theoretical investigations are indispensable.

The top quark production associated with a W boson, i.e. tW -channel, as shown in the leading order (LO) Feynman diagrams in figure 1, can be used to probe the coupling between the W boson and the top quark, including the Cabibbo-Kobayashi-Maskawa matrix element V_{tb} . The ATLAS and CMS collaborations at the CERN large hadron collider (LHC) have already observed the signal of this process based on the data accumulated at center-of-mass energies of 7, 8, 13 TeV [2–10]. So far, only the data recorded in 2016, corresponding to 35.9 fb^{-1} integrated luminosity, have been taken into account in the public analyses, and the uncertainty of the measured cross section is about 11% [11]. It is expected that the measured cross section of this process will become more precise as more data are going to be analysed in the future.

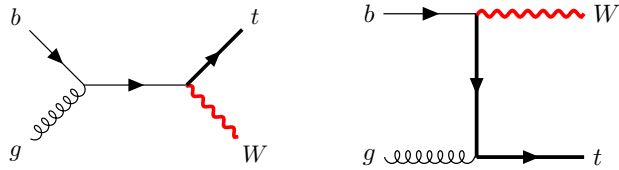


Figure 1. Leading order Feynman diagrams for $gb \rightarrow tW$.

To match the accuracy of the experimental measurements, the theoretical predictions must include higher-order radiative effects in the perturbative theories. Since the strong coupling is the largest among the three interactions relevant for fundamental particles, the QCD corrections are the dominant contribution. The next-to-leading order (NLO) corrections have been obtained for stable tW final state [12–15] as well as the process including the decay of the top quark and the W boson [16]. The approximate next-to-next-to-next-to-leading order total cross section has been derived by expanding the threshold resummation formula [17–20]. The all-order corrections induced by soft gluons are considered in [21]. The effect of parton shower has been studied in [22–24].

However, the complete next-to-next-to-leading order (NNLO) QCD corrections have not been obtained yet, though a small fraction of the two-loop master integrals have recently been computed analytically [25, 26]. To obtain these corrections, the double-real, real-virtual and double-virtual corrections should be calculated independently and collected together in the end to provide an infrared (IR) finite prediction. In arranging the cancellation of IR divergences, the phase space slicing method [27] is one of the promising approaches. Above the slicing cut, which can be the transverse momentum of the tW system or the N-jettiness variable [28] in this process, only the NLO divergence appears and it is appropriate to use some automatic packages to perform the calculation. In this part, it is mandatory to consider the interference with the top quark pair production with a top quark decay $\bar{t} \rightarrow W\bar{b}$ in order to provide a well-defined perturbative prediction. Different schemes have been proposed to tackle this issue [29]. Below the slicing cut, a factorization of the cross section to several simpler functions holds at the leading power in the ratio of the cut over the center-of-mass energy. Expanding the factorization formula to certain orders in the strong coupling gives the required fixed-order contributions. As one of the ingredients in the factorization formula, the N-jettiness soft function has been calculated at NNLO by two of the authors [30, 31]. The missing part is the NNLO hard function, which demands the calculation of one-loop squared amplitudes and the interference between two-loop and tree-level amplitudes. In this paper, we present the result of the former.

This paper is organized as follows. In section 2, we show the kinematics of tW production and the notations used in the following sections. Then we describe the details in calculating the one-loop squared amplitudes in section 3, including the γ_5 scheme, renormalization procedure, and the infrared divergences cancellation. In section 4 we discuss the approximation method by expansion in m_W^2 . Conclusions are made in section 5.

2 Kinematics and notations

The process $g(k_1)b(k_2) \rightarrow W(k_3)t(k_4)$ contains two massive final states with different masses. For the external particles, there are on-shell conditions $k_1^2 = 0, k_2^2 = 0, k_3^2 = m_W^2$ and $k_4^2 = (k_1 + k_2 - k_3)^2 = m_t^2$. The Mandelstam variables are defined as

$$s = (k_1 + k_2)^2, \quad t = (k_1 - k_3)^2, \quad u = (k_2 - k_3)^2 \quad (2.1)$$

with $s + t + u = m_W^2 + m_t^2$.

The LO matrix element is

$$\mathcal{M}^{(0)} = \frac{e g_s t_{4,2}^a}{\sqrt{2} \sin \theta_W} \left(\frac{\bar{u}(k_4) \not{\epsilon}_3^* P_L (\not{k}_3 + \not{k}_4) \not{\epsilon}_1 u(k_2)}{s} + \frac{\bar{u}(k_4) \not{\epsilon}_1 (\not{k}_2 - \not{k}_3 + m_t) \not{\epsilon}_3^* P_L u(k_2)}{u - m_t^2} \right), \quad (2.2)$$

where $t_{4,2}^a$ is the generator of the color SU(3) gauge group inserted between the top quark and the bottom quark. ϵ_1^μ and $\epsilon_3^{*\mu}$ are the polarization vectors for the gluon and W boson, respectively. P_L is the projection operator to the left-handed quarks.

The polarization summation over all physical polarization states for the W boson and the gluon is

$$\sum_i \epsilon_i^{*\mu}(k_3) \epsilon_i^\nu(k_3) = -g^{\mu\nu} + \frac{k_3^\mu k_3^\nu}{m_W^2} \quad (2.3)$$

and

$$\sum_i \epsilon_i^\mu(k_1) \epsilon_i^{*\nu}(k_1) = -g^{\mu\nu} + \frac{k_1^\mu n^\nu + k_1^\nu n^\mu}{k_1 \cdot n}, \quad (2.4)$$

respectively. Here n is a light-like four-vector. Consequently, the ghost field is not needed in the external state in the loop amplitudes. In practice, we can simply use

$$\sum_i \epsilon_i^\mu(k_1) \epsilon_i^{*\nu}(k_1) = -g^{\mu\nu}. \quad (2.5)$$

due to the Ward identity¹. As a result, we obtain the LO amplitude squared

$$\begin{aligned} \overline{|\mathcal{M}^{(0)}|^2} &= \frac{e^2 g_s^2 C_F}{32 \sin^2 \theta_W s (u - m_t^2)^2 m_W^2} \left[m_t^8 - m_t^6 (2s + u) + m_t^4 (-2m_W^4 - 2m_W^2 u + (s + u)^2) \right. \\ &\quad + m_t^2 (4m_W^6 - 2m_W^4 u + 2m_W^2 (s^2 - su + 2u^2) - u(s + u)^2) \\ &\quad \left. - 2m_W^2 u (2m_W^4 - 2m_W^2 (s + u) + s^2 + u^2) \right], \quad (2.6) \end{aligned}$$

where the factors from spin and color average in the initial states have been included.

The LO hadronic cross section for tW production at the LHC is

$$\sigma = \int_0^1 dx_1 dx_2 \frac{1}{2s} \int d\Phi_2 \left[f_{g/p}(x_1, \mu_f) f_{b/p}(x_2, \mu_f) \overline{|\mathcal{M}^{(0)}|^2} + (x_1 \leftrightarrow x_2) \right], \quad (2.7)$$

¹In order to check the Ward identity, all the external particles are required to be physical. If there are more than two gluons in the external state, e.g., $gb \rightarrow Wtg$, it is not appropriate to use eq.(2.5) for gluons.

where $d\Phi_2$ is the Lorentz invariant two-body phase space, and $f_{i/p}(x, \mu_f)$ is the parton distribution function at the factorization scale μ_f .

In order to obtain the complete NNLO QCD corrections to this process, we need to obtain one-loop virtual corrections to $\mathcal{M}_{gb \rightarrow Wt}$ up to $\mathcal{O}(\epsilon^2)$, two-loop virtual corrections to $\mathcal{M}_{gb \rightarrow Wt}$ up to $\mathcal{O}(\epsilon^0)$, one-loop virtual corrections to $\mathcal{M}_{gb \rightarrow Wt+j}$ up to $\mathcal{O}(\epsilon^0)$ ², and tree-level $\mathcal{M}_{gb \rightarrow Wt+jj}$. In this paper, we focus on the first contribution, leaving the others and the combination of all contributions after phase space integration to the future work.

3 One-loop calculation

3.1 Bare loop amplitudes

We generate all the one-loop virtual diagrams as well as the diagrams with counterterms by FeynArts [32]. The corresponding amplitudes can be written down automatically and manipulated by FeynCalc [33]. We do not keep the polarization information at the moment and focus only on amplitude squared, i.e., we calculate the interference between the one-loop diagrams and tree-level or one-loop diagrams. All the Lorentz indices are contracted after spin sums, and therefore the loop integrals appear in the form of scalar integrals, though there may be some loop momenta in the numerators. The spin and polarization information may be useful if one wants to study the kinematic distribution of the decay products of the top quark and the W boson. This can be obtained by using the spinor-helicity formalism for the external states after decay, as in [16] for the NLO corrections, or by replacing the polarization vector of specific helicities by a linear combination of external momenta [34]. Our calculation can be readily extended to the helicity amplitudes because they share the same master integrals as the spin-summed amplitudes.

We have chosen the anticommuting γ_5 scheme following ref. [35] to calculate the traces in the squared amplitude. In this scheme, it is easy to deal with the traces with two (or more generally even number of) γ_5 matrices in our case due to the anticommutativity property. In the trace with a single (or more generally odd number of) γ_5 , since the cyclicity in traces has been sacrificed, we choose the Wtb vertex in the amplitude as a *reading point*, i.e. the starting vertex in a trace. The non-vanishing trace with one γ_5 would contribute an anti-symmetric $\varepsilon_{\mu\nu\rho\sigma}$ tensor to each term in the result. Its Lorentz indices should contract only with those of the external momenta in the spin summed amplitude squared, given that there exists only one fermion line. Since only three independent momenta are involved in tW production process, the traces with one γ_5 would vanish at the end.

Then we use two different methods to reduce all the scalar integrals in the squared amplitude to a set of basis integrals, called master integrals. In the first method, the reduction is performed following the Passarino-Veltman procedure [36], and the master integrals can be found from the literature [37] or calculated by Package-X [38] up to $\mathcal{O}(\epsilon^0)$. They can also be evaluated up to higher orders in ϵ using the AMFlow package [39]. In the other method, we use integration-by-parts (IBP) technique to derive relations among the scalar integrals

²It is not necessary to compute this part up to $\mathcal{O}(\epsilon^2)$ because the scattering amplitude reduces to $\mathcal{M}_{gb \rightarrow Wt}$ when the integration of three-body phase space develops a pole in ϵ .

and carry out the reduction using FIRE [40]. The master integrals are calculated using the method of differential equations [41, 42]. After transforming the differential equations to a canonical form [43], the solutions can be readily obtained up to any orders in ϵ . It has been checked analytically that both methods lead to the same results for the interference of one-loop and tree-level amplitudes. For the one-loop squared amplitudes, the coefficients of ϵ^{-4} and ϵ^{-3} coincide in analytical form, while the coefficients of ϵ^{-2} , ϵ^{-1} and ϵ^0 agree numerically. We also notice that there are more master integrals using Passarino-Veltman reduction than IBP relations. The coefficients of the master integrals in the former contain no divergences, while those in the latter do. These differences indicate that the agreement between the two methods is highly non-trivial. In the following, we present more details about the IBP method.

We find that all the master integrals in the one-loop diagrams could be expressed in terms of three families of master integrals as:

$$\begin{aligned} I_{n_1, n_2, n_3, n_4}^1 &= \int \mathcal{D}^D q_1 \frac{1}{D_1^{n_1} D_2^{n_2} D_3^{n_3} D_4^{n_4}}, \\ I_{n_1, n_2, n_3, n_4}^2 &= \int \mathcal{D}^D q_1 \frac{1}{D_1^{n_1} D_2^{n_2} D_5^{n_3} D_4^{n_4}}, \\ I_{n_1, n_2, n_3, n_4}^3 &= \int \mathcal{D}^D q_1 \frac{1}{D_1^{n_1} D_6^{n_2} D_3^{n_3} D_4^{n_4}} \end{aligned}$$

with

$$\mathcal{D}^D q_1 = \frac{(m_t^2)^\epsilon}{i\pi^{D/2}\Gamma(1+\epsilon)} d^D q_1 \quad (3.1)$$

and

$$\begin{aligned} D_1 &= -q_1^2, \\ D_2 &= -(q_1 + k_2)^2, \\ D_3 &= -(q_1 + k_1 + k_2)^2, \\ D_4 &= -(q_1 + k_4)^2 + m_t^2, \\ D_5 &= -(q_1 + k_2 - k_3)^2 + m_t^2, \\ D_6 &= -(q_1 + k_1)^2. \end{aligned} \quad (3.2)$$

We will present the details for the calculation of the first family in the text, but leave the second family to the appendix A. The third family can be related to the first using $k_1 \leftrightarrow k_2$, and thus we will not present the results for the master integrals in it.

For the squared one-loop amplitude, the reduction of any general integral to master integrals can be carried out as the traditional two-loop integrals. It is interesting to notice that additional Lorentz invariant combinations, such as $(q_1 \cdot q_2)^3$ with q_2 being another loop momentum, can appear in the squared amplitude after summing the polarizations of the vector bosons. But they do not appear in the master integrals. As a consequence, we need the product of one integral in any of the above families and another in complex conjugate form.

The canonical basis of the first family is chosen to be

$$\begin{aligned}
M_1 &= \epsilon I_{0,0,0,2}^1, \\
M_2 &= \epsilon t I_{0,1,0,2}^1, \\
M_3 &= \epsilon m_W^2 I_{0,0,1,2}^1, \\
M_4 &= \epsilon s I_{1,0,2,0}^1, \\
M_5 &= \epsilon^2 \sqrt{(s - (m_W - m_t)^2)} \sqrt{(s - (m_W + m_t)^2)} I_{1,0,1,1}^1, \\
M_6 &= \epsilon^2 s (t - m_t^2) I_{1,1,1,1}^1.
\end{aligned} \tag{3.3}$$

To rationalize the roots, we define the variables x, y, z via

$$\begin{aligned}
s &= m_t^2 \frac{(x+z)(1+xz)}{x}, \\
t &= y m_t^2, \\
m_W &= z m_t.
\end{aligned} \tag{3.4}$$

The master integrals in eq.(3.3) satisfy the differential equation

$$d\mathbf{M}(x, y, z; \epsilon) = \epsilon (d\tilde{A}) \mathbf{M}(x, y, z; \epsilon) \tag{3.5}$$

with

$$d\tilde{A} = \sum_{i=1}^{12} R_i d\ln(l_i). \tag{3.6}$$

The arguments l_i of this $d\ln$ form encode all the dependence of the differential equations on the kinematics, are called the *alphabet*, consisting of the following letters,

$$\begin{aligned}
l_1 &= x, & l_2 &= x + 1, \\
l_3 &= x - 1, & l_4 &= x + z, \\
l_5 &= x z + 1, & l_6 &= x y + z, \\
l_7 &= x z + y, & l_8 &= y, \\
l_9 &= y - 1, & l_{10} &= y - z^2, \\
l_{11} &= z, & l_{12} &= z^2 - 1.
\end{aligned} \tag{3.7}$$

R_i are rational matrices, given by

$$R_1 = \begin{pmatrix} 0 & 0 & 0 & 0 & 0 & 0 \\ 0 & 0 & 0 & 0 & 0 & 0 \\ 0 & 0 & 0 & 0 & 0 & 0 \\ 0 & 0 & 0 & 1 & 0 & 0 \\ 1 & 0 & 0 & -1 & 0 & 0 \\ 1 & 2 & 0 & 0 & 0 & 0 \end{pmatrix}, \quad R_2 = \begin{pmatrix} 0 & 0 & 0 & 0 & 0 & 0 \\ 0 & 0 & 0 & 0 & 0 & 0 \\ 0 & 0 & 0 & 0 & 0 & 0 \\ 0 & 0 & 0 & 0 & 0 & 0 \\ 0 & 0 & 0 & 0 & 2 & 0 \\ 0 & 0 & 0 & 0 & 0 & 0 \end{pmatrix}, \quad R_3 = \begin{pmatrix} 0 & 0 & 0 & 0 & 0 & 0 \\ 0 & 0 & 0 & 0 & 0 & 0 \\ 0 & 0 & 0 & 0 & 0 & 0 \\ 0 & 0 & 0 & 0 & 0 & 0 \\ 0 & 0 & 0 & 0 & 2 & 0 \\ 0 & 0 & 0 & 0 & 0 & 0 \end{pmatrix},$$

$$\begin{aligned}
R_4 &= \begin{pmatrix} 0 & 0 & 0 & 0 & 0 & 0 \\ 0 & 0 & 0 & 0 & 0 & 0 \\ 0 & 0 & 0 & 0 & 0 & 0 \\ 0 & 0 & 0 & -1 & 0 & 0 \\ -1 & 0 & -2 & 1 & -2 & 0 \\ -\frac{1}{2} & 0 & -1 & 1 & -1 & -1 \end{pmatrix}, \quad R_5 = \begin{pmatrix} 0 & 0 & 0 & 0 & 0 & 0 \\ 0 & 0 & 0 & 0 & 0 & 0 \\ 0 & 0 & 0 & 0 & 0 & 0 \\ 0 & 0 & 0 & -1 & 0 & 0 \\ 1 & 0 & 2 & -1 & -2 & 0 \\ -\frac{1}{2} & 0 & -1 & 1 & 1 & -1 \end{pmatrix}, \\
R_6 &= \begin{pmatrix} 0 & 0 & 0 & 0 & 0 & 0 \\ 0 & 0 & 0 & 0 & 0 & 0 \\ 0 & 0 & 0 & 0 & 0 & 0 \\ 0 & 0 & 0 & 0 & 0 & 0 \\ 0 & 0 & 0 & 0 & 0 & 0 \\ -\frac{1}{2} & -2 & 1 & -1 & 1 & 1 \end{pmatrix}, \quad R_7 = \begin{pmatrix} 0 & 0 & 0 & 0 & 0 & 0 \\ 0 & 0 & 0 & 0 & 0 & 0 \\ 0 & 0 & 0 & 0 & 0 & 0 \\ 0 & 0 & 0 & 0 & 0 & 0 \\ 0 & 0 & 0 & 0 & 0 & 0 \\ -\frac{1}{2} & -2 & 1 & -1 & -1 & 1 \end{pmatrix}, \\
R_8 &= \begin{pmatrix} 0 & 0 & 0 & 0 & 0 & 0 \\ 0 & 1 & 0 & 0 & 0 & 0 \\ 0 & 0 & 0 & 0 & 0 & 0 \\ 0 & 0 & 0 & 0 & 0 & 0 \\ 0 & 0 & 0 & 0 & 0 & 0 \\ 0 & 0 & 0 & 0 & 0 & 0 \end{pmatrix}, \quad R_9 = \begin{pmatrix} 0 & 0 & 0 & 0 & 0 & 0 \\ -1 & -2 & 0 & 0 & 0 & 0 \\ 0 & 0 & 0 & 0 & 0 & 0 \\ 0 & 0 & 0 & 0 & 0 & 0 \\ 0 & 0 & 0 & 0 & 0 & 0 \\ 1 & 2 & 0 & 0 & 0 & -2 \end{pmatrix}, \\
R_{10} &= \begin{pmatrix} 0 & 0 & 0 & 0 & 0 & 0 \\ 0 & 0 & 0 & 0 & 0 & 0 \\ 0 & 0 & 0 & 0 & 0 & 0 \\ 0 & 0 & 0 & 0 & 0 & 0 \\ 0 & 0 & 0 & 0 & 0 & 0 \\ 0 & 2 & -2 & 0 & 0 & 0 \end{pmatrix}, \quad R_{11} = \begin{pmatrix} 0 & 0 & 0 & 0 & 0 & 0 \\ 0 & 0 & 0 & 0 & 0 & 0 \\ 0 & 0 & 2 & 0 & 0 & 0 \\ 0 & 0 & 0 & 0 & 0 & 0 \\ 0 & 0 & 0 & 0 & 2 & 0 \\ 0 & 0 & 0 & 0 & 0 & 0 \end{pmatrix}, \quad R_{12} = \begin{pmatrix} 0 & 0 & 0 & 0 & 0 & 0 \\ 0 & 0 & 0 & 0 & 0 & 0 \\ -1 & 0 & -2 & 0 & 0 & 0 \\ 0 & 0 & 0 & 0 & 0 & 0 \\ 0 & 0 & 0 & 0 & 0 & 0 \\ 1 & 0 & 2 & 0 & 0 & 0 \end{pmatrix}.
\end{aligned}$$

In order to solve the above differential equations, we need to specify the boundary conditions. The integrals M_1 and M_4 are simple enough so that one can get the analytical results with full dependence on ϵ from direct computation. Since all the one-loop integrals we encounter do not have any branch cut at the kinematic points corresponding to $t = 0$, $m_W = 0$, $s = (m_t + m_W)^2$, and $ut = m_t^2 m_W^2$, they are regular without any singularity at these kinematic points. The boundary condition of M_2 is obtained using the fact that it is regular at $t = 0$. Explicitly, the coefficient of $1/t$ in the differential equation, which is a linear combination of some master integrals, is vanishing. Similarly, the boundary conditions of M_3 , M_5 and M_6 are derived from the regular condition at $m_W = 0$, $s = (m_t + m_W)^2$ and $ut = m_t^2 m_W^2$, respectively.

Since the letters are just polynomials in x, y, z , we can solve the differential equation recursively using the boundaries discussed above and write the final result in terms of the multiple polylogarithms [44], which are defined as $G(x) \equiv 1$ and

$$G_{a_1, a_2, \dots, a_n}(x) \equiv \int_0^x \frac{dt}{t - a_1} G_{a_2, \dots, a_n}(t), \quad (3.8)$$

$$G_{\vec{0}_n}(x) \equiv \frac{1}{n!} \ln^n x. \quad (3.9)$$

The dimension of the vector (a_1, a_2, \dots, a_n) is usually called the transcendental *weight* of the multiple polylogarithm. We need multiple polylogarithms of at most transcendental weight four in the one-loop squared amplitudes.

3.2 Renormalization

The loop amplitude computed above contains ultra-violet (UV) and IR divergences. The UV divergences cancel with the contribution from counter-terms, arising from the renormalization of the couplings, masses and field strength.

In general, there are two methods to calculate the contribution of counter-terms. In one method, the bare Lagrangian is used to generate the Feynman rules and the loop amplitudes, and the external wave function renormalization is taken into account according to the Lehmann–Symanzik–Zimmermann (LSZ) reduction formula. We introduce the renormalization factor Z_2^g, Z_2^b, Z_2^t for the gluon field, bottom quark field and top quark field, respectively, by defining the renormalized fields as $\psi_{\text{bare}} = Z_2^{1/2} \psi_r, A_{\text{bare}}^\mu = (Z_2^g)^{1/2} A_r^\mu$. We do not consider the renormalization of the W boson field since we focus only on QCD corrections. Then the bare masses and couplings in the result should be replaced by the physical masses and couplings. The relation between the bare top quark mass $m_{t,\text{bare}}$ and the physical mass m_t is $m_{t,\text{bare}} = Z_m^t m_t$. The strong coupling α_s is renormalized in the $\overline{\text{MS}}$ scheme through the identity $\alpha_s^{\text{bare}} C_\epsilon = \mu^{2\epsilon} \alpha_s^{\text{ren}} Z_{\alpha_s}$ ³ with $C_\epsilon = (4\pi e^{-\gamma_E})^\epsilon$. The perturbative expansion of these renormalization factors is listed in the appendix B. As a result, the UV renormalized scattering amplitude up to two loops is

$$\begin{aligned} \mathcal{M}_{\text{ren}} &= \mathcal{M}_{\text{bare}}^{(0)} + \frac{\alpha_s^{\text{bare}}}{4\pi} (\mathcal{M}_{\text{bare}}^{(1)} + \mathcal{M}_{\text{C.T.}}^{(1)}) + \left(\frac{\alpha_s^{\text{bare}}}{4\pi} \right)^2 (\mathcal{M}_{\text{bare}}^{(2)} + \mathcal{M}_{\text{C.T.}}^{(2)}) \\ &= \mathcal{M}_{\text{ren}}^{(0)} + \frac{\alpha_s}{4\pi} \mathcal{M}_{\text{ren}}^{(1)} + \left(\frac{\alpha_s}{4\pi} \right)^2 \mathcal{M}_{\text{ren}}^{(2)}, \end{aligned} \quad (3.10)$$

where $\mathcal{M}_{\text{bare}}$ is the bare amplitude and $\mathcal{M}_{\text{C.T.}}$ denotes the amplitude whenever higher-order results of the renormalization factors are used. In the first line, we express the results in terms of bare quantities, while the second line contains only renormalized ones. There is not a one-to-one correspondence between the two lines, e.g., the third term in the second line could receive contributions from the second term in the first line.

The other method is to use the Lagrangian in terms of renormalized fields and couplings, which includes new counter-term vertices. The top quark two-point counter-term vertex is described by $i[\not{p}(Z_2^t - 1) - (Z_2^t Z_m^t - 1)m_t]$. The combination of the top quark propagator and the two-point counter-terms now becomes

$$\frac{i(Z_2^t)^{-1}}{\not{p} - m_t} \left(1 + \frac{m_t \delta Z_m^t}{\not{p} - m_t} + \frac{(m_t \delta Z_m^t)^2}{(\not{p} - m_t)^2} + \dots \right), \quad (3.11)$$

where we have used the notation $\delta Z \equiv Z - 1$. The omitted terms do not contribute to an NNLO calculation. Similar expressions can be obtained for the massless bottom quark by just neglecting all the mass terms. The gluon and quark three-point counter-term vertex is given by a multiplicative factor $\delta_1^q = Z_{g_s} Z_2^q (Z_2^g)^{1/2} - 1, q = t, b$. The Wtb

³For simplicity, we use α_s to denote α_s^{ren} everywhere in the paper.

counter-term vertex has a factor $\delta_1^W = (Z_2^t)^{1/2}(Z_2^b)^{1/2} - 1$. At two loops, we would also need the gluon two-point and three-point counter-terms. Furthermore, no wave function renormalization factors are needed in the LSZ formula because physical fields have been employed. Therefore, the renormalized scattering amplitude up to NNLO is given by

$$\begin{aligned}\mathcal{M}_{\text{ren}} &= \mathcal{M}_{\text{ren}}^{(0)} + \frac{\alpha_s}{4\pi}(\mathcal{M}_{\text{loop}}^{(1)} + \mathcal{M}_{\text{C.T.}}^{(1)}) + \left(\frac{\alpha_s}{4\pi}\right)^2 (\mathcal{M}_{\text{loop}}^{(2)} + \mathcal{M}_{\text{C.T.}}^{(2)}) \\ &= \mathcal{M}_{\text{ren}}^{(0)} + \frac{\alpha_s}{4\pi}\mathcal{M}_{\text{ren}}^{(1)} + \left(\frac{\alpha_s}{4\pi}\right)^2 \mathcal{M}_{\text{ren}}^{(2)},\end{aligned}\tag{3.12}$$

where $\mathcal{M}_{\text{loop}}$ is the loop amplitude and $\mathcal{M}_{\text{C.T.}}$ denotes the amplitude with counter-term vertices inserted in a diagram anywhere possible except for the external legs. The UV divergences cancel between $\mathcal{M}_{\text{loop}}^{(i)}$ and $\mathcal{M}_{\text{C.T.}}^{(i)}$, and thus there is a one-to-one correspondence between the two lines in the above equation.

The two renormalization methods are equivalent, which can be understood by observing the cancellation of the wave function renormalization factors in eq.(3.11) and those in the combination of tree-level and counter-terms vertices⁴. As a result, only the renormalization factors associated with the external particles, as well as δZ_{α_s} and δZ_m^t , should be considered.

In eq.(3.12), we have used a superscript to denote the order in α_s for the perturbative expansion of the amplitude. Notice that $\mathcal{M}_{\text{C.T.}}^{(2)}$ contains not only the tree-level diagrams with counter-terms at α_s^2 but also the one-loop diagrams with counter-terms at α_s . Since the one-loop integrals contain up to $1/\epsilon^2$ poles, we need the counter-terms at $\mathcal{O}(\alpha_s)$ up to $\mathcal{O}(\epsilon^2)$ in $\mathcal{M}_{\text{C.T.}}^{(2)}$. They are also needed when we calculate the squared amplitude, e.g., $\mathcal{M}_{\text{loop}}^{(1)}(\mathcal{M}_{\text{C.T.}}^{(1)})^*$.

3.3 Infrared divergences

After taking into account the contribution of counter-terms, the UV divergences disappear. But there are still IR divergences. These will cancel with the corresponding contribution of real corrections⁵ in the prediction for a physical observable. This cancellation should be checked analytically before performing any reasonable numerical computation. Though the real correction is out of the scope of this paper, we can make a non-trivial check based on the understanding of the factorization property of amplitudes in the IR limit. More precisely, it has been proven that the UV renormalized amplitude can be written in the form

$$\mathcal{M}_{\text{ren}} = \mathbf{Z}\mathcal{M}_{\text{fin}},\tag{3.13}$$

where all the IR divergences are encoded in the factor \mathbf{Z} and the remainder is finite as $\epsilon \rightarrow 0$ [45–48]. Following our convention, both the \mathbf{Z} factor and the finite part have an expansion in α_s ,

$$\mathbf{Z} = 1 + \frac{\alpha_s}{4\pi}\mathbf{Z}^{(1)} + \left(\frac{\alpha_s}{4\pi}\right)^2 \mathbf{Z}^{(2)} + \dots,$$

⁴An analogous equation to eq.(3.11) for the gluon propagator including counter-term vertices can be obtained in the Landau gauge.

⁵At hadron colliders, renormalization of the parton distribution function is also needed.

$$\mathcal{M}_{\text{fin}} = \mathcal{M}_{\text{fin}}^{(0)} + \frac{\alpha_s}{4\pi} \mathcal{M}_{\text{fin}}^{(1)} + \left(\frac{\alpha_s}{4\pi}\right)^2 \mathcal{M}_{\text{fin}}^{(2)} + \dots \quad (3.14)$$

Then it is ready to get

$$\begin{aligned} \mathcal{M}_{\text{fin}}^{(0)} &= \mathcal{M}_{\text{ren}}^{(0)}, \\ \mathcal{M}_{\text{fin}}^{(1)} &= \mathcal{M}_{\text{ren}}^{(1)} - \mathbf{Z}^{(1)} \mathcal{M}_{\text{ren}}^{(0)}, \\ \mathcal{M}_{\text{fin}}^{(2)} &= \mathcal{M}_{\text{ren}}^{(2)} + ((\mathbf{Z}^{(1)})^2 - \mathbf{Z}^{(2)}) \mathcal{M}_{\text{ren}}^{(0)} - \mathbf{Z}^{(1)} \mathcal{M}_{\text{ren}}^{(1)}. \end{aligned} \quad (3.15)$$

The factor \mathbf{Z} has been computed up to two-loop order for a general process with massive colored particles [47–49], and to three-loop order for single top production [50]. In the present paper, we are interested in the one-loop squared amplitudes,

$$\left| \mathcal{M}_{\text{fin}}^{(1)} \right|^2 = \left| \mathcal{M}_{\text{ren}}^{(1)} \right|^2 + \left| \mathbf{Z}^{(1)} \mathcal{M}_{\text{ren}}^{(0)} \right|^2 - (\mathbf{Z}^{(1)} \mathcal{M}_{\text{ren}}^{(0)} \mathcal{M}_{\text{ren}}^{(1)*} + \mathbf{Z}^{(1)*} \mathcal{M}_{\text{ren}}^{(0)*} \mathcal{M}_{\text{ren}}^{(1)}), \quad (3.16)$$

where the \mathbf{Z} factor at one loop is given by

$$\begin{aligned} \mathbf{Z}^{(1)} &= - (C_A + C_F) \frac{\gamma_{\text{cusp}}^{(0)}}{4\epsilon^2} + \frac{\gamma_g^{(0)} + \gamma_b^{(0)} + \gamma_t^{(0)}}{2\epsilon} \\ &\quad + \frac{\gamma_{\text{cusp}}^{(0)}}{4\epsilon} \left(-C_A \ln \frac{\mu^2}{-s} - C_A \ln \frac{\mu m_t}{m_t^2 - u} + (C_A - 2C_F) \ln \frac{\mu m_t}{m_t^2 - t} \right). \end{aligned} \quad (3.17)$$

The anomalous dimensions γ_{cusp} , γ_g , γ_b and γ_t can be found in the appendix of ref. [51]. Notice that we have chosen such a factorization scheme that \mathbf{Z} does not have any finite part, which corresponds to the $\overline{\text{MS}}$ scheme. The presence of double poles in $\mathbf{Z}^{(1)}$ requires the squared amplitudes $\mathcal{M}_{\text{ren}}^{(0)} \mathcal{M}_{\text{ren}}^{(1)*}$ and $\mathcal{M}_{\text{ren}}^{(1)} \mathcal{M}_{\text{ren}}^{(0)*}$ to be calculated up to $\mathcal{O}(\epsilon^2)$ because this could contribute to the $\mathcal{O}(\epsilon^0)$ part in $\left| \mathcal{M}_{\text{fin}}^{(1)} \right|^2$.

The second term on the right hand side of eq.(3.16) contains ϵ^{-4} poles, which should cancel with those in the first and third terms. As a result, we can check the coefficient of ϵ^{-4} in $\left| \mathcal{M}_{\text{ren}}^{(1)} \right|^2$ and in turn that in $\left| \mathcal{M}_{\text{bare}}^{(1)} \right|^2$ analytically, given that the result with $\mathcal{M}_{\text{C.T.}}^{(1)}$ is easier to obtain. Similar cancellation has been checked analytically for the coefficient of ϵ^{-3} . However, it is nontrivial to check the cancellation of the coefficients of ϵ^{-2} and ϵ^{-1} analytically because the $\mathcal{O}(\epsilon^0)$ and $\mathcal{O}(\epsilon^1)$ parts of $\mathcal{M}_{\text{bare}}^{(1)}$ would get involved. Instead, we confine the cancellation to be numerical with high precision. In figure 2, we present our numerical results for these coefficients. In the plots, we have used the parameters β_t and $\cos \theta$ that are very suitable to describe the kinematics of the collision process in a finite range. More specifically, the top quark momentum is written as $k_4^\mu = E_t(1, \beta_t \sin \theta \cos \phi, \beta_t \sin \theta \sin \phi, \beta_t \cos \theta)$ in the center-of-mass frame of the incoming partons, where $\beta_t = \sqrt{1 - m_t^2/E_t^2}$ measures the velocity of the top quark and θ is the angle between the initial-state gluon and the final-state top quark.

It can be seen that the magnitudes of the coefficients span over several orders, especially growing or decreasing very fast as $\beta_t \rightarrow 1$. We have checked that the cancellation of these coefficients with the other parts in eq.(3.16) happens at the level of at least eight digits over

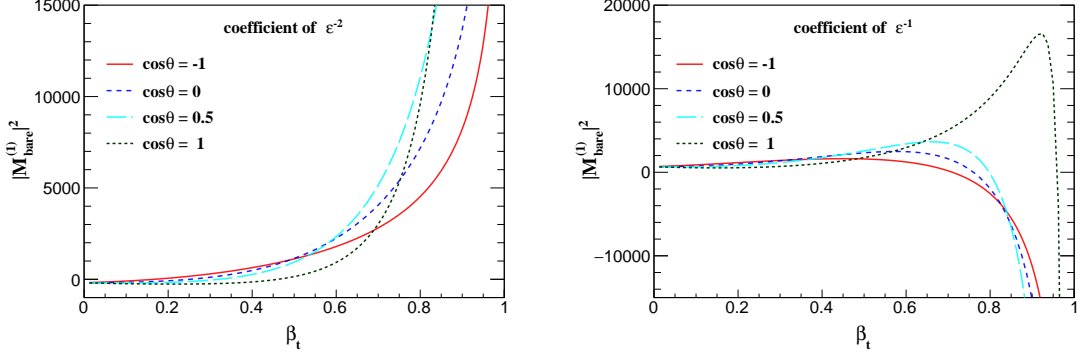


Figure 2. The coefficients of ϵ^{-2} (left) and ϵ^{-1} (right) in the bare loop squared amplitude as a function of β_t with several fixed values of $\cos\theta$. The red, blue, cyan and dark green lines are for $\cos\theta = -1$, $\cos\theta = 0$, $\cos\theta = 0.5$ and $\cos\theta = 1$, respectively. We fix the mass ratio $m_W/m_t = \sqrt{3/14}$ and extract a global factor $e^2 g_s^2 / \sin^2 \theta_W$. The renormalization scale is set to be $\mu = m_t$.

almost the whole range of β_t and $\cos\theta$ ⁶. Actually, it is not an easy task to achieve this. The main obstacle is the precise calculation of the very lengthy coefficients of the master integrals in the squared amplitudes, which contain high powers of s , t and u variables. And they are represented in terms of β_t and $\cos\theta$ as

$$\begin{aligned}
s &= m_W^2 + \frac{1 + \beta_t^2}{1 - \beta_t^2} m_t^2 + \frac{2m_t}{1 - \beta_t^2} \sqrt{m_W^2 + \beta_t^2(m_t^2 - m_W^2)}, \\
t &= m_t^2 - \frac{1 + \beta_t \cos\theta}{1 - \beta_t^2} \left(m_t^2 + m_t \sqrt{m_W^2 + \beta_t^2(m_t^2 - m_W^2)} \right), \\
u &= m_t^2 - \frac{1 - \beta_t \cos\theta}{1 - \beta_t^2} \left(m_t^2 + m_t \sqrt{m_W^2 + \beta_t^2(m_t^2 - m_W^2)} \right). \quad (3.18)
\end{aligned}$$

In our calculation, for each phase space point $(\beta_t, \cos\theta)$, we first compute the above s , t and u variables in high precision floating number, e.g., by keeping over 20 digits, and then transform them to rational numbers before inserting them to the expressions of the coefficients of the master integrals. We have observed a strong cancellation among different terms in each coefficient for small or large β_t . The cancellation of all the divergences in eq.(3.16), either analytically or numerically, is an important check of the whole calculation.

At last, we turn to the finite part. Figure 3 shows the numerical result of $|\mathcal{M}_{\text{fin}}^{(1)}|^2$ as a function of β_t and $\cos\theta$. It can be seen that the finite one-loop squared amplitude increases remarkably when β_t becomes large. The reason is that the mass of the top quark becomes vanishing in the limit $\beta_t \rightarrow 1$ ⁷. New collinear divergences, which have been regularized by m_t and appeared as logarithms of $1 - \beta_t^2$, will appear. From the right plot of figure 3, we observe that the finite part is insensitive to $\cos\theta$ when β_t is small. But the dependence of the finite part on $\cos\theta$ becomes stronger with the increasing of β_t .

⁶We do not cover the phase space points with $\beta_t = 1$, where the coefficients become divergent due to new collinear singularities. But in practice, we will not reach such a point since the top quark mass is not vanishing (or the collider energy is limited).

⁷Or one may think that it is the region where the collider energy goes to infinity. This does not affect the discussion on the divergences.

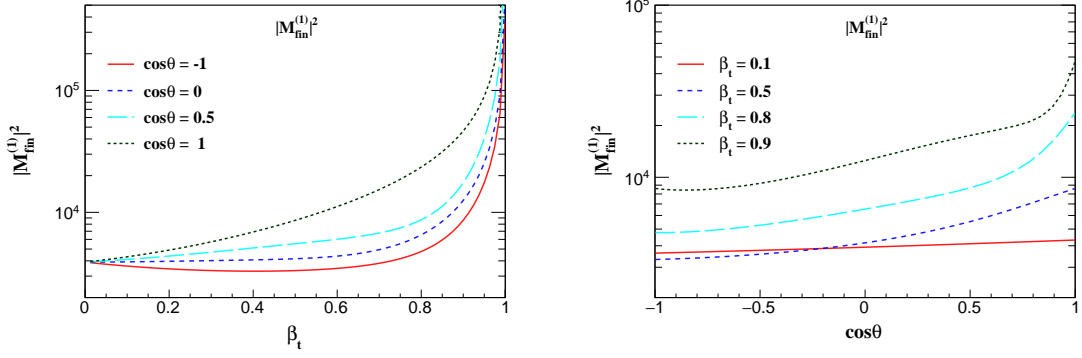


Figure 3. $|\mathcal{M}_{\text{fin}}^{(1)}|^2$ with fixed $\cos\theta$ (left) and β_t (right). The other parameters are set the same as figure 2.

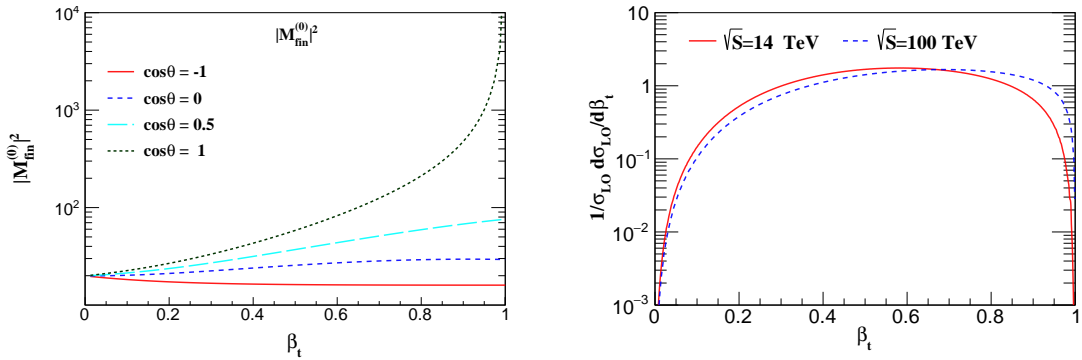


Figure 4. The LO squared amplitude (left) and normalized cross section (right) as a function of β_t . In the left plot, the other parameters are set the same as figure 2. In the right plot, the renormalization and factorization scales are set to be m_t . The red and blue lines correspond to the collider energy $\sqrt{S} = 14$ and 100 TeV, respectively, while β_t is calculated in partonic central-of-mass frame.

For comparison, we present the LO squared amplitude in the left plot in figure 4. We see that it is divergent only in the limit $\beta_t \rightarrow 1$ and $\cos\theta \rightarrow 1$. This is the region when the t -channel propagator in figure 1 becomes on-shell. Notice that the two kinds of divergences in the limit $\beta_t \rightarrow 1$ are different, because the collinear divergences discussed above can appear for any values of $\cos\theta$. In practice, both of them are not harmful to the hadronic cross section due to the suppression of parton distribution function in the large β_t region. After phase space integration, the LO partonic cross section is proportional to $\ln(1 - \beta_t)$, but the hadronic cross section is vanishing as $\beta_t \rightarrow 1$, as shown in the right plot of figure 4. This means that the suppression of the parton distribution function surpasses the enhancement of the partonic cross section. This is also the case at higher orders, since only $\ln^n(1 - \beta_t)$ can appear in the partonic cross section. From the right plot of figure 4, we also observe that the suppression becomes weaker with the increasing of the collider energy.

To see the impact of the one-loop amplitude squared, we show the ratio R of $|\mathcal{M}_{\text{fin}}^{(1)}|^2$ to $|\mathcal{M}_{\text{fin}}^{(0)}|^2$ in figure 5. We find that the ratio R changes slowly away from the region of $\beta_t \rightarrow 1$ or $\cos\theta \rightarrow 1$ and grows dramatically for large β_t . For the phase space with $\beta_t < 0.9$,

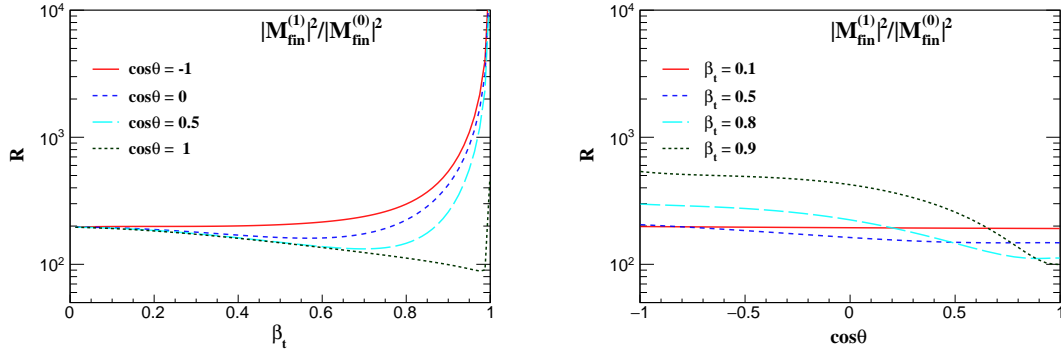


Figure 5. The ratio of $|\mathcal{M}_{\text{fin}}^{(1)}|^2$ to $|\mathcal{M}_{\text{fin}}^{(0)}|^2$ as a function of β_t (left plot) and $\cos\theta$ (right plot).

which is the dominant region contributing to a real collider process, the corrections from one-loop amplitude squared are at the percent level, if the strong coupling is taken to be around 0.1.

4 Expansion in m_W^2

The complexity of the loop amplitude mounts up prominently as the number of the independent scales increases. There are four independent scales in the process of tW production, i.e., m_t^2, m_W^2, s, t . It is beneficial to computation if one can expand the amplitude in one scale. For the process we are interested in, setting $m_W = 0$ does not bring any new IR divergences over the full phase space due to the massive top quark propagator. Therefore, it is feasible to take the Taylor series expansion of the amplitude with respect to m_W^2 . After setting $m_W = 0$, one only needs to deal with integrals depending on three variables, i.e., s, t, m_t^2 . As a consequence, both the IBP reduction and calculation of master integrals are simplified considerably. The square roots in eq.(3.3) will disappear, and thus the one-loop results become easier. Furthermore, at two-loop level, small mass expansion can make the calculation of some master integrals that would contain elliptic functions when keeping finite m_W possible in terms of multiple polylogarithms. A similar method has been adopted in the analytic calculation of the two-loop $gg \rightarrow HH$ amplitude [52, 53].

Given that the analytic result is still out of reach, we want to apply the method of Taylor expansion in m_W^2 to compute the approximate two-loop amplitude of tW production. In this section, we demonstrate the validity of this method using the exact one-loop result we have obtained. As shown in eq.(2.2), the LO scattering amplitude contains the denominator s and $u - m_t^2$. One reasonable choice is to keep the invariant s and u and replace $t \rightarrow -s - u + m_t^2 + m_W^2$ before expanding the amplitudes in a series of m_W^2 .

Regarding the calculation of master integrals, we explicitly show the expansion of I_{n_1, n_2, n_3, n_4}^i defined in eq.(3.1),

$$I_{n_1, n_2, n_3, n_4}^i(s, u, m_W^2, m_t^2) = \sum_{n=0}^{\infty} \frac{(m_W^2)^n}{n!} \left. \frac{\partial^n I_{n_1, n_2, n_3, n_4}^i}{\partial (m_W^2)^n} \right|_{m_W^2=0}. \quad (4.1)$$

The differential operator of m_W^2 should be written in a form that can directly act on a loop integral,

$$\frac{\partial}{\partial(m_W^2)} = (c_1 k_1 + c_2 k_2 + c_3 k_3) \cdot \frac{\partial}{\partial k_3} \quad (4.2)$$

with the coefficients

$$\begin{aligned} c_1 &= \frac{u(-m_W^2 + 2s + u) + m_t^2(m_W^2 - u)}{2s(u(-m_W^2 + s + u) + m_t^2(m_W^2 - u))}, \\ c_2 &= \frac{(u - m_t^2)(-m_t^2 + s + u)}{2s(u(-m_W^2 + s + u) + m_t^2(m_W^2 - u))}, \\ c_3 &= \frac{m_t^2 - u}{2(u(-m_W^2 + s + u) + m_t^2(m_W^2 - u))}. \end{aligned} \quad (4.3)$$

Notice that these c_i coefficients should be expanded further in a series of m_W^2 before taking the limit $m_W^2 \rightarrow 0$ in eq.(4.1).

Actually, this differential operators can act not only on the master integrals, but also on the whole squared amplitude. However, we do not apply them to the variable m_W^2 in the summation of the polarizations of the W boson in eq.(2.3). This denominator arises because the longitudinal polarization state of the W boson has a different coupling to quarks from the transverse ones. If we separate the contribution from different polarizations and express the coupling of the longitudinal polarization state and quarks in terms of the top quark Yukawa coupling, there is no such m_W^2 factor in the denominator, according to the Goldstone boson equivalence theorem [54, 55]. This property can also be seen if we use Feynman-'t Hooft gauge to sum the polarizations of the W boson

$$\sum_i \epsilon_i^{*\mu}(k_3) \epsilon_i^\nu(k_3) = -g^{\mu\nu} \quad (4.4)$$

and add the contribution of the Goldstone boson production diagram, which does not involve a polarization sum.

After applying the differential operator to master integrals, each term in the series of m_W^2 can be expressed as a linear combination of scalar integrals. Then we reduce them to a set of master integrals with $m_W = 0$. The advantages of the expansion come from two aspects. First, the number of these master integrals is less than that before expansion. Second, the analytic computation is easier to perform. For example, the square root in eq.(3.3) does not exist at $m_W = 0$. Further, the set of master integrals is the same at all orders in the expansion, therefore no additional computation cost needs to be paid if we want to obtain the result of even higher orders in the expansion of m_W^2 in principle.

Figure 6 demonstrates the accuracy of the m_W expansion, taking the real part of $I_{1,1,1,1}^1$ as an example. We compare the expanded results for the coefficients of ϵ^i with $i = -2, \dots, 2$ to the exact ones. As more higher orders in m_W^2 are included, the expansion approximation becomes better. The difference between the expansion up to $\mathcal{O}(m_W^6)$ and the exact values are at the permille level or better. We also find that expansion series converge faster in the larger β_t region. This is reasonable because the expansion parameter m_W^2/s is generally

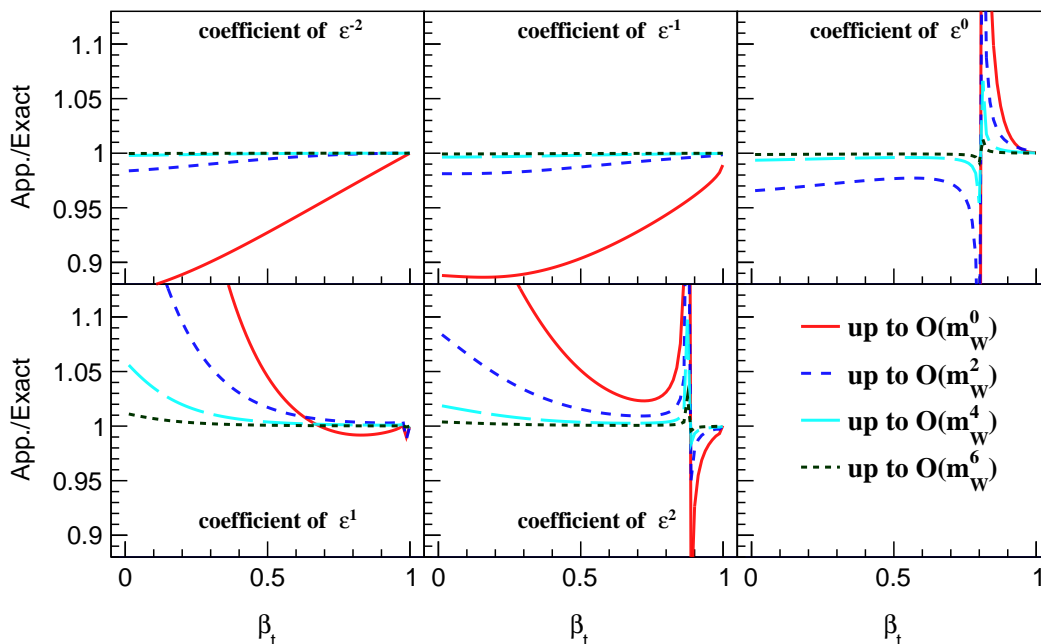


Figure 6. The accuracy of m_W expansion for the real part of one-loop integral $I_{1,1,1,1}^1$ up to ϵ^2 and $\mathcal{O}(m_W^6)$ with $\cos\theta = 0.5$. The red, blue, cyan and dark green lines stand for the expansions up to $\mathcal{O}(m_W^0)$, $\mathcal{O}(m_W^2)$, $\mathcal{O}(m_W^4)$, and $\mathcal{O}(m_W^6)$, respectively. The notable divergences in the plots appear because the exact results almost vanish around that specific value of β_t .

smaller in this region. In the plots, there are some regions where the curves seem to be divergent. We have checked the absolute values of both the expanded and exact results, and found that they are almost vanishing in these regions.

Then we consider the expansion of the squared amplitudes. As mentioned above, the differential operator can be applied to the squared amplitude. This can be done just after creating the amplitude from the Feynman diagrams. Firstly, we replace k_4 by $k_1 + k_2 - k_3$ everywhere. Secondly, we contract the Lorentz indices in the spin summed squared amplitude. Thirdly, we apply the differential operator in eq.(4.2) to the squared amplitude⁸, and reduce all the scalar integrals to master integrals with $k_3^2 = 0$. However, we will use another method. Since we have expressed the squared amplitude as a combination of the master integrals and their coefficients, we only have to expand the coefficients in m_W^2 , given that the master integrals have been expanded as discussed above. Figure 7 shows $|\mathcal{M}_{\text{bare}}^{(1)}|^2$ and their expansions in m_W^2 with $\cos\theta = 0.5$ as a function of β_t . It can be seen that the differences between the exact results and the expanded ones up to $\mathcal{O}(m_W^4)$ are already notably small. The corrections of order m_W^6 are negligible.

We have also tried to expand only all the master integrals but keep the exact form of the coefficients of the master integrals. One may expect that this approach would have a better approximation to the exact result. On the contrary, we find that the expansion is worse,

⁸The differential operators must also be applied to the polarization sum of the W boson except for the denominator m_W^2 .

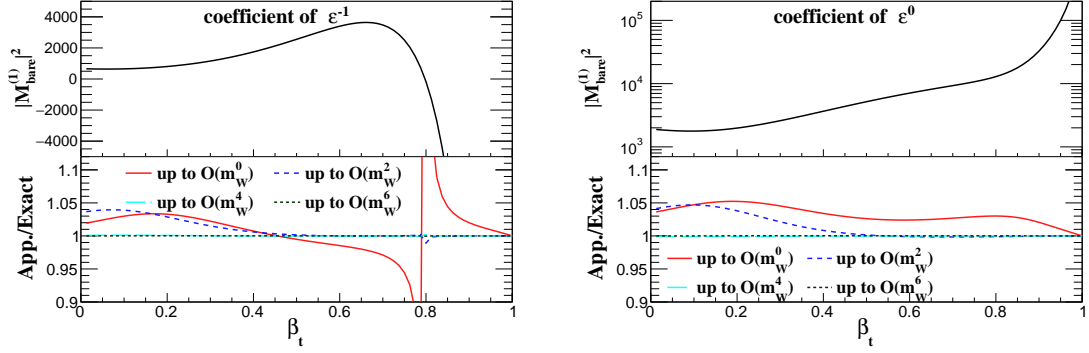


Figure 7. The numerical results for the coefficients of ϵ^{-1} (left) and ϵ^0 (right) in $|\mathcal{M}_{\text{bare}}^{(1)}|^2$ and their expansions in m_W with $\cos\theta = 0.5$ as a function of β_t . The upper panels show the exact results of one-loop squared amplitudes. The lower panels show the ratios between the m_W expansions and the exact results. The color scheme is the same as in figure 6.

sometimes even seems divergent in small β_t regions. As mentioned before, the coefficients contain a lot of terms, in which the powers of the kinematic variables are very high. For specific values of the kinematic variables, the cancellation among these terms happens over about ten digits. In the expansion in m_W^2 , this cancellation holds at each order. If the coefficients contain higher orders in m_W^2 than the master integrals, the cancellation is not complete. As a result, the deviation between the expanded results and the exact ones may be large.

5 Conclusions

The precise prediction of tW associated production at a hadron collider is important to study the properties of the top quark and the W boson. We have computed the analytic results for the one-loop squared amplitudes for this process using canonical differential equations. The renormalized amplitude squared has up to ϵ^{-4} poles, which have been checked against the general infrared structures predicted by anomalous dimensions. The finite part gives rise to about a few percent corrections compared to the corresponding LO results. We also investigate how to obtain approximated results using the method of expansion in m_W^2 , and find that the expanded results up to $\mathcal{O}(m_W^4)$ are already accurate enough to present the exact results. It is promising to apply this expansion method in calculating the interference of two-loop and tree level amplitudes.

Acknowledgements

This work was supported in part by the National Science Foundation of China under grant No.12175048, No.12005117, No.12147154 and No.12075251. The work of L.D. and J.W. was also supported by the Taishan Scholar Foundation of Shandong province (tsqn201909011).

A Rational matrices and boundary conditions for the second integral family

The canonical basis of the second family consists of

$$\begin{aligned}
N_1 &= \epsilon I_{0,0,0,2}^2, \\
N_2 &= \epsilon t I_{0,1,0,2}^2, \\
N_3 &= \epsilon u I_{1,0,2,0}^2, \\
N_4 &= \epsilon m_W^2 I_{0,1,2,0}^2, \\
N_5 &= \epsilon^2 (u - m_t^2) I_{1,0,1,1}^2, \\
N_6 &= \epsilon^2 (t - m_W^2) I_{0,1,1,1}^2, \\
N_7 &= \epsilon^2 (t - m_t^2)(u - m_t^2) I_{1,1,1,1}^2,
\end{aligned} \tag{A.1}$$

which satisfy the differential equation

$$d\mathbf{N}(y, z, v; \epsilon) = \epsilon (d\tilde{B}) \mathbf{N}(y, z, v; \epsilon) \tag{A.2}$$

with

$$d\tilde{B} = \sum_{i=1}^{10} P_i d\ln(L_i). \tag{A.3}$$

The letters are given by

$$\begin{aligned}
L_1 &= y, & L_2 &= v, \\
L_3 &= 1 + z^2 - y - v, & L_4 &= z^2, \\
L_5 &= y - 1, & L_6 &= v - 1, \\
L_7 &= z^2 - 1, & L_8 &= y - z^2, \\
L_9 &= v - z^2, & L_{10} &= yv - z^2
\end{aligned} \tag{A.4}$$

with $v \equiv \frac{u}{m_t^2}$ and y, z defined in eq.(3.4). The rational matrices P_i are

$$\begin{aligned}
P_1 &= \begin{pmatrix} 0 & 0 & 0 & 0 & 0 & 0 & 0 & 0 \\ 0 & 1 & 0 & 0 & 0 & 0 & 0 & 0 \\ 0 & 0 & 0 & 0 & 0 & 0 & 0 & 0 \\ 0 & 0 & 0 & 0 & 0 & 0 & 0 & 0 \\ 0 & 0 & 0 & 0 & 0 & 0 & 0 & 0 \\ 0 & 1 & 0 & 0 & 0 & 0 & 0 & 0 \\ 0 & 0 & 0 & 0 & 0 & 0 & 0 & 0 \end{pmatrix}, & P_2 &= \begin{pmatrix} 0 & 0 & 0 & 0 & 0 & 0 & 0 & 0 \\ 0 & 0 & 0 & 0 & 0 & 0 & 0 & 0 \\ 0 & 0 & 1 & 0 & 0 & 0 & 0 & 0 \\ 0 & 0 & 0 & 0 & 0 & 0 & 0 & 0 \\ 0 & 0 & 1 & 0 & 0 & 0 & 0 & 0 \\ 0 & 0 & 0 & 0 & 0 & 0 & 0 & 0 \\ 0 & 0 & 0 & 0 & 0 & 0 & 0 & 0 \end{pmatrix}, \\
P_3 &= \begin{pmatrix} 0 & 0 & 0 & 0 & 0 & 0 & 0 & 0 \\ 0 & 0 & 0 & 0 & 0 & 0 & 0 & 0 \\ 0 & 0 & 0 & 0 & 0 & 0 & 0 & 0 \\ 0 & 0 & 0 & 0 & 0 & 0 & 0 & 0 \\ 0 & 0 & 0 & 0 & 0 & 0 & 0 & 0 \\ 0 & 0 & 0 & 0 & 0 & 0 & 0 & 0 \\ -\frac{1}{2} & -1 & -1 & 1 & 1 & 1 & 1 & 1 \end{pmatrix}, & P_4 &= \begin{pmatrix} 0 & 0 & 0 & 0 & 0 & 0 & 0 & 0 \\ 0 & 0 & 0 & 0 & 0 & 0 & 0 & 0 \\ 0 & 0 & 0 & 0 & 0 & 0 & 0 & 0 \\ 0 & 0 & 0 & 1 & 0 & 0 & 0 & 0 \\ 0 & 0 & 0 & 0 & 0 & 0 & 0 & 0 \\ 0 & 0 & 0 & -1 & 0 & 0 & 0 & 0 \\ 0 & 0 & 0 & 0 & 0 & 0 & 0 & 0 \end{pmatrix},
\end{aligned}$$

$$\begin{aligned}
P_5 &= \begin{pmatrix} 0 & 0 & 0 & 0 & 0 & 0 & 0 \\ -1 & -2 & 0 & 0 & 0 & 0 & 0 \\ 0 & 0 & 0 & 0 & 0 & 0 & 0 \\ 0 & 0 & 0 & 0 & 0 & 0 & 0 \\ 0 & 0 & 0 & 0 & 0 & 0 & 0 \\ 0 & 0 & 0 & 0 & 0 & 0 & 0 \\ 0 & 0 & 0 & 0 & 0 & 0 & -2 \end{pmatrix}, & P_6 &= \begin{pmatrix} 0 & 0 & 0 & 0 & 0 & 0 & 0 \\ 0 & 0 & 0 & 0 & 0 & 0 & 0 \\ -1 & 0 & -2 & 0 & 0 & 0 & 0 \\ 0 & 0 & 0 & 0 & 0 & 0 & 0 \\ 0 & 0 & 0 & 0 & 0 & 0 & 0 \\ 0 & 0 & 0 & 0 & 0 & 0 & 0 \\ 0 & 0 & 0 & 0 & 0 & 0 & -2 \end{pmatrix}, \\
P_7 &= \begin{pmatrix} 0 & 0 & 0 & 0 & 0 & 0 & 0 \\ 0 & 0 & 0 & 0 & 0 & 0 & 0 \\ 0 & 0 & 0 & 0 & 0 & 0 & 0 \\ -1 & 0 & 0 & -2 & 0 & 0 & 0 \\ 0 & 0 & 0 & 0 & 0 & 0 & 0 \\ 0 & 0 & 0 & 0 & 0 & 0 & 0 \\ 0 & 0 & 0 & 0 & 0 & 0 & 0 \\ 1 & 0 & 0 & 2 & 0 & 0 & 0 \end{pmatrix}, & P_8 &= \begin{pmatrix} 0 & 0 & 0 & 0 & 0 & 0 & 0 \\ 0 & 0 & 0 & 0 & 0 & 0 & 0 \\ 0 & 0 & 0 & 0 & 0 & 0 & 0 \\ 0 & 0 & 0 & 0 & 0 & 0 & 0 \\ 0 & 0 & 0 & 0 & 0 & 0 & 0 \\ 0 & 0 & 0 & 0 & 0 & 0 & 0 \\ 0 & 0 & 0 & 0 & 0 & 0 & 0 \\ 0 & 2 & 0 & -2 & 0 & 0 & 0 \end{pmatrix}, \\
P_9 &= \begin{pmatrix} 0 & 0 & 0 & 0 & 0 & 0 & 0 \\ 0 & 0 & 0 & 0 & 0 & 0 & 0 \\ 0 & 0 & 0 & 0 & 0 & 0 & 0 \\ 0 & 0 & 0 & 0 & 0 & 0 & 0 \\ 0 & 0 & 0 & 0 & 0 & 0 & 0 \\ 0 & 0 & 0 & 0 & 0 & 0 & 0 \\ 0 & 0 & 0 & 0 & 0 & 0 & 0 \\ 0 & 0 & 2 & -2 & 0 & 0 & 0 \end{pmatrix}, & P_{10} &= \begin{pmatrix} 0 & 0 & 0 & 0 & 0 & 0 & 0 \\ 0 & 0 & 0 & 0 & 0 & 0 & 0 \\ 0 & 0 & 0 & 0 & 0 & 0 & 0 \\ 0 & 0 & 0 & 0 & 0 & 0 & 0 \\ 0 & 0 & 0 & 0 & 0 & 0 & 0 \\ 0 & 0 & 0 & 0 & 0 & 0 & 0 \\ 0 & 0 & 0 & 0 & 0 & 0 & 0 \\ -\frac{1}{2} & -1 & -1 & 1 & -1 & -1 & 1 \end{pmatrix}. \tag{A.5}
\end{aligned}$$

The boundaries of these basis integrals are fixed by either direct computation (for N_1) or regular conditions (for $N_2 \sim N_7$). More explicitly, N_2, \dots, N_7 are regular at $t = 0, u = 0, m_W = 0, u = m_t^2, t = m_W^2, s = 0$, without any singularity, respectively.

B Perturbative expansion of renormalization factors

The strong coupling α_s is renormalized in the $\overline{\text{MS}}$ scheme. The renormalization factor is given by [56, 57]

$$Z_{\alpha_s} = 1 - \frac{\alpha_s}{4\pi} \frac{\beta_0}{\epsilon} + \left(\frac{\alpha_s}{4\pi}\right)^2 \left(\frac{\beta_0^2}{\epsilon^2} - \frac{\beta_1}{2\epsilon}\right) + \mathcal{O}(\alpha_s^3) \tag{B.1}$$

with

$$\begin{aligned}
\beta_0 &= \frac{11}{3}C_A - \frac{4}{3}T_F n_f, \\
\beta_1 &= \frac{34}{3}C_A^2 - \frac{20}{3}C_A T_F n_f - 4C_F T_F n_f. \tag{B.2}
\end{aligned}$$

In QCD, we have $C_A = 3, C_F = 4/3, T_F = 1/2$. Here n_f is the total number of quark flavors, including both massless and massive quarks. As a result, the running strong coupling satisfies the renormalization equation

$$\frac{d\alpha_s}{d \ln \mu} = -2\alpha_s \left(\frac{\alpha_s}{4\pi} \beta_0 + \left(\frac{\alpha_s}{4\pi}\right)^2 \beta_1 + \dots \right). \tag{B.3}$$

In our calculation, the wave function renormalization factors are determined by the on-shell renormalization condition for the external particles, and have been expanded in a series of α_s . The first three orders are given by [58–60]

$$\begin{aligned}
Z_2^g &= 1 + \left(\frac{\alpha_s}{4\pi}\right) T_F n_h D_\epsilon \left(-\frac{4}{3\epsilon}\right) + \left(\frac{\alpha_s}{4\pi}\right)^2 T_F n_h D_\epsilon^2 \left[C_F \left(-\frac{2}{\epsilon} - 15\right) + C_A \left(\frac{35}{9\epsilon^2} - \frac{5}{2\epsilon} \right. \right. \\
&\quad \left. \left. + \frac{13}{12} - \frac{11\pi^2}{27}\right) + T_F \left(-\frac{16}{9\epsilon^2} n_l + \frac{4\pi^2}{27} n_f\right) + \frac{4}{3} \beta_0 \ln\left(\frac{\mu^2}{m_t^2}\right) \left(-\frac{1}{\epsilon} + \frac{1}{2} \ln\left(\frac{\mu^2}{m_t^2}\right)\right) \right], \\
Z_2^b &= 1 + \left(\frac{\alpha_s}{4\pi}\right)^2 C_F T_F n_h \left(\frac{1}{\epsilon} + 2 \ln\frac{\mu^2}{m_t^2} - \frac{5}{6}\right), \\
Z_2^t &= 1 + \left(\frac{\alpha_s}{4\pi}\right) C_F D_\epsilon \left(-\frac{3}{\epsilon} - 4 - 8\epsilon - 16\epsilon^2\right) + \left(\frac{\alpha_s}{4\pi}\right)^2 C_F D_\epsilon^2 \left[T_F n_h \left(\frac{1}{\epsilon} + \frac{947}{18} - 5\pi^2\right) \right. \\
&\quad \left. + T_F n_l \left(-\frac{2}{\epsilon^2} + \frac{11}{3\epsilon} + \frac{113}{6} + \frac{5\pi^2}{3}\right) + C_F \left(\frac{9}{2\epsilon^2} + \frac{51}{4\epsilon} + \frac{433}{8} - 13\pi^2 \right. \right. \\
&\quad \left. \left. + 16\pi^2 \ln 2 - 24\zeta(3)\right) + C_A \left(\frac{11}{2\epsilon^2} - \frac{127}{12\epsilon} - \frac{1705}{24} + \frac{49\pi^2}{12} - 8\pi^2 \ln 2 + 12\zeta(3)\right) \right. \\
&\quad \left. + \beta_0 \ln\left(\frac{\mu^2}{m_t^2}\right) \left(-\frac{3}{\epsilon} - 4 + \frac{3}{2} \ln\left(\frac{\mu^2}{m_t^2}\right)\right) \right], \\
Z_m^t &= 1 + \left(\frac{\alpha_s}{4\pi}\right) C_F D_\epsilon \left(-\frac{3}{\epsilon} - 4 - 8\epsilon - 16\epsilon^2\right) + \left(\frac{\alpha_s}{4\pi}\right)^2 C_F D_\epsilon^2 \left[T_F n_h \left(-\frac{2}{\epsilon^2} + \frac{5}{3\epsilon} + \frac{143}{6} \right. \right. \\
&\quad \left. \left. - \frac{7\pi^2}{3}\right) + T_F n_l \left(-\frac{2}{\epsilon^2} + \frac{5}{3\epsilon} + \frac{71}{6} + \frac{5\pi^2}{3}\right) + C_F \left(\frac{9}{2\epsilon^2} + \frac{45}{4\epsilon} + \frac{199}{8} - 5\pi^2 \right. \right. \\
&\quad \left. \left. + 8\pi^2 \ln 2 - 12\zeta(3)\right) + C_A \left(\frac{11}{2\epsilon^2} - \frac{97}{12\epsilon} - \frac{1111}{24} + \frac{5\pi^2}{12} - 4\pi^2 \ln 2 + 6\zeta(3)\right) \right. \\
&\quad \left. + \beta_0 \ln\left(\frac{\mu^2}{m_t^2}\right) \left(-\frac{3}{\epsilon} - 4 + \frac{3}{2} \ln\left(\frac{\mu^2}{m_t^2}\right)\right) \right] \tag{B.4}
\end{aligned}$$

with

$$D_\epsilon \equiv \frac{\Gamma(1+\epsilon)}{e^{-\gamma_E \epsilon}} \left(\frac{\mu^2}{m_t^2}\right)^\epsilon. \tag{B.5}$$

We have used n_h (n_l) to denote the number of massive (massless) quarks, though in our case it is natural to set $n_h = 1$. Notice that Z_2^t and Z_m^t are the same at $\mathcal{O}(\alpha_s)$ if we do not distinguish the IR and UV divergences in dimensional regularization, but not the same at higher orders [61].

References

- [1] CDF collaboration, T. Aaltonen et al., *High-precision measurement of the W boson mass with the CDF II detector*, *Science* **376** (2022) 170–176.
- [2] ATLAS collaboration, G. Aad et al., *Evidence for the associated production of a W boson and a top quark in ATLAS at $\sqrt{s} = 7$ TeV*, *Phys. Lett.* **B716** (2012) 142–159, [1205.5764].

- [3] ATLAS collaboration, G. Aad et al., *Measurement of the production cross-section of a single top quark in association with a W boson at 8 TeV with the ATLAS experiment*, *JHEP* **01** (2016) 064, [[1510.03752](#)].
- [4] ATLAS collaboration, M. Aaboud et al., *Measurement of the cross-section for producing a W boson in association with a single top quark in pp collisions at $\sqrt{s} = 13$ TeV with ATLAS*, *JHEP* **01** (2018) 063, [[1612.07231](#)].
- [5] ATLAS collaboration, M. Aaboud et al., *Measurement of differential cross-sections of a single top quark produced in association with a W boson at $\sqrt{s} = 13$ TeV with ATLAS*, *Eur. Phys. J.* **C78** (2018) 186, [[1712.01602](#)].
- [6] ATLAS collaboration, G. Aad et al., *Measurement of single top-quark production in association with a W boson in the single-lepton channel at $\sqrt{s} = 8$ TeV with the ATLAS detector*, *Eur. Phys. J. C* **81** (2021) 720, [[2007.01554](#)].
- [7] CMS collaboration, S. Chatrchyan et al., *Evidence for associated production of a single top quark and W boson in pp collisions at $\sqrt{s} = 7$ TeV*, *Phys. Rev. Lett.* **110** (2013) 022003, [[1209.3489](#)].
- [8] CMS collaboration, S. Chatrchyan et al., *Observation of the associated production of a single top quark and a W boson in pp collisions at $\sqrt{s} = 8$ TeV*, *Phys. Rev. Lett.* **112** (2014) 231802, [[1401.2942](#)].
- [9] CMS collaboration, A. M. Sirunyan et al., *Measurement of the production cross section for single top quarks in association with W bosons in proton-proton collisions at $\sqrt{s} = 13$ TeV*, *JHEP* **10** (2018) 117, [[1805.07399](#)].
- [10] CMS collaboration, A. Tumasyan et al., *Observation of tW production in the single-lepton channel in pp collisions at $\sqrt{s} = 13$ TeV*, *JHEP* **11** (2021) 111, [[2109.01706](#)].
- [11] A. S. Rodríguez, *Inclusive and differential cross-sections measurements in the single top tW e-mu channel with CMS*, *PoS EPS-HEP2021* (2022) 444, [[2112.08976](#)].
- [12] W. T. Giele, S. Keller and E. Laenen, *QCD corrections to W boson plus heavy quark production at the Tevatron*, *Phys. Lett.* **B372** (1996) 141–149, [[hep-ph/9511449](#)].
- [13] S. Zhu, *Next-to-leading order QCD corrections to $bg \rightarrow tW^-$ at CERN large hadron collider*, *Phys. Lett.* **B524** (2002) 283–288, [[hep-ph/0109269](#)].
- [14] Q.-H. Cao, *Demonstration of One Cutoff Phase Space Slicing Method: Next-to-Leading Order QCD Corrections to the tW Associated Production in Hadron Collision*, [0801.1539](#).
- [15] P. Kant, O. M. Kind, T. Kintscher, T. Lohse, T. Martini, S. Mölbitz et al., *HatHor for single top-quark production: Updated predictions and uncertainty estimates for single top-quark production in hadronic collisions*, *Comput. Phys. Commun.* **191** (2015) 74–89, [[1406.4403](#)].
- [16] J. M. Campbell and F. Tramontano, *Next-to-leading order corrections to Wt production and decay*, *Nucl. Phys.* **B726** (2005) 109–130, [[hep-ph/0506289](#)].
- [17] N. Kidonakis, *Single top production at the Tevatron: Threshold resummation and finite-order soft gluon corrections*, *Phys. Rev.* **D74** (2006) 114012, [[hep-ph/0609287](#)].
- [18] N. Kidonakis, *Two-loop soft anomalous dimensions for single top quark associated production with a W^- or H^-* , *Phys. Rev.* **D82** (2010) 054018, [[1005.4451](#)].
- [19] N. Kidonakis, *Soft-gluon corrections for tW production at N^3 LO*, *Phys. Rev.* **D96** (2017) 034014, [[1612.06426](#)].

- [20] N. Kidonakis and N. Yamanaka, *Higher-order corrections for tW production at high-energy hadron colliders*, *JHEP* **05** (2021) 278, [[2102.11300](#)].
- [21] C. S. Li, H. T. Li, D. Y. Shao and J. Wang, *Momentum-space threshold resummation in tW production at the LHC*, *JHEP* **06** (2019) 125, [[1903.01646](#)].
- [22] S. Frixione, E. Laenen, P. Motylinski, B. R. Webber and C. D. White, *Single-top hadroproduction in association with a W boson*, *JHEP* **07** (2008) 029, [[0805.3067](#)].
- [23] E. Re, *Single-top Wt -channel production matched with parton showers using the POWHEG method*, *Eur. Phys. J.* **C71** (2011) 1547, [[1009.2450](#)].
- [24] T. Ježo, J. M. Lindert, P. Nason, C. Oleari and S. Pozzorini, *An NLO+PS generator for $t\bar{t}$ and Wt production and decay including non-resonant and interference effects*, *Eur. Phys. J.* **C76** (2016) 691, [[1607.04538](#)].
- [25] L.-B. Chen and J. Wang, *Analytic two-loop master integrals for tW production at hadron colliders: I **, *Chin. Phys. C* **45** (2021) 123106, [[2106.12093](#)].
- [26] M.-M. Long, R.-Y. Zhang, W.-G. Ma, Y. Jiang, L. Han, Z. Li et al., *Two-loop master integrals for the single top production associated with W boson*, [2111.14172](#).
- [27] S. Catani and M. Grazzini, *An NNLO subtraction formalism in hadron collisions and its application to Higgs boson production at the LHC*, *Phys. Rev. Lett.* **98** (2007) 222002, [[hep-ph/0703012](#)].
- [28] I. W. Stewart, F. J. Tackmann and W. J. Waalewijn, *N -Jettiness: An Inclusive Event Shape to Veto Jets*, *Phys. Rev. Lett.* **105** (2010) 092002, [[1004.2489](#)].
- [29] F. Demartin, B. Maier, F. Maltoni, K. Mawatari and M. Zaro, *tWH associated production at the LHC*, *Eur. Phys. J.* **C77** (2017) 34, [[1607.05862](#)].
- [30] H. T. Li and J. Wang, *Next-to-Next-to-Leading Order N -Jettiness Soft Function for One Massive Colored Particle Production at Hadron Colliders*, *JHEP* **02** (2017) 002, [[1611.02749](#)].
- [31] H. T. Li and J. Wang, *Next-to-next-to-leading order N -jettiness soft function for tW production*, *Phys. Lett.* **B784** (2018) 397–404, [[1804.06358](#)].
- [32] T. Hahn, *Generating Feynman diagrams and amplitudes with FeynArts 3*, *Comput. Phys. Commun.* **140** (2001) 418–431, [[hep-ph/0012260](#)].
- [33] V. Shtabovenko, R. Mertig and F. Orellana, *FeynCalc 9.3: New features and improvements*, *Comput. Phys. Commun.* **256** (2020) 107478, [[2001.04407](#)].
- [34] L. Chen, *A prescription for projectors to compute helicity amplitudes in D dimensions*, *Eur. Phys. J. C* **81** (2021) 417, [[1904.00705](#)].
- [35] J. G. Korner, D. Kreimer and K. Schilcher, *A Practicable $\gamma(5)$ scheme in dimensional regularization*, *Z. Phys. C* **54** (1992) 503–512.
- [36] G. Passarino and M. J. G. Veltman, *One Loop Corrections for $e^+ e^-$ Annihilation Into $\mu^+ \mu^-$ in the Weinberg Model*, *Nucl. Phys. B* **160** (1979) 151–207.
- [37] R. K. Ellis and G. Zanderighi, *Scalar one-loop integrals for QCD*, *JHEP* **02** (2008) 002, [[0712.1851](#)].
- [38] H. H. Patel, *Package-X: A Mathematica package for the analytic calculation of one-loop integrals*, *Comput. Phys. Commun.* **197** (2015) 276–290, [[1503.01469](#)].

- [39] X. Liu and Y.-Q. Ma, *AMFlow: a Mathematica package for Feynman integrals computation via Auxiliary Mass Flow*, [2201.11669](#).
- [40] R. N. Lee, *Presenting LiteRed: a tool for the Loop InTEgrals REDuction*, [1212.2685](#).
- [41] A. V. Kotikov, *Differential equations method: New technique for massive Feynman diagrams calculation*, *Phys. Lett.* **B254** (1991) 158–164.
- [42] A. V. Kotikov, *Differential equation method: The Calculation of N point Feynman diagrams*, *Phys. Lett.* **B267** (1991) 123–127.
- [43] J. M. Henn, *Multiloop integrals in dimensional regularization made simple*, *Phys. Rev. Lett.* **110** (2013) 251601, [[1304.1806](#)].
- [44] A. B. Goncharov, *Multiple polylogarithms, cyclotomy and modular complexes*, *Math. Res. Lett.* **5** (1998) 497–516, [[1105.2076](#)].
- [45] T. Becher and M. Neubert, *Infrared singularities of scattering amplitudes in perturbative QCD*, *Phys. Rev. Lett.* **102** (2009) 162001, [[0901.0722](#)].
- [46] T. Becher and M. Neubert, *On the Structure of Infrared Singularities of Gauge-Theory Amplitudes*, *JHEP* **06** (2009) 081, [[0903.1126](#)].
- [47] T. Becher and M. Neubert, *Infrared singularities of QCD amplitudes with massive partons*, *Phys. Rev. D* **79** (2009) 125004, [[0904.1021](#)].
- [48] A. Ferroglia, M. Neubert, B. D. Pecjak and L. L. Yang, *Two-loop divergences of scattering amplitudes with massive partons*, *Phys. Rev. Lett.* **103** (2009) 201601, [[0907.4791](#)].
- [49] A. Mitov, G. F. Sterman and I. Sung, *Computation of the Soft Anomalous Dimension Matrix in Coordinate Space*, *Phys. Rev. D* **82** (2010) 034020, [[1005.4646](#)].
- [50] N. Kidonakis, *Soft anomalous dimensions for single-top production at three loops*, *Phys. Rev. D* **99** (2019) 074024, [[1901.09928](#)].
- [51] H. T. Li, C. S. Li, D. Y. Shao, L. L. Yang and H. X. Zhu, *Top quark pair production at small transverse momentum in hadronic collisions*, *Phys. Rev. D* **88** (2013) 074004, [[1307.2464](#)].
- [52] X. Xu and L. L. Yang, *Towards a new approximation for pair-production and associated-production of the Higgs boson*, *JHEP* **01** (2019) 211, [[1810.12002](#)].
- [53] G. Wang, Y. Wang, X. Xu, Y. Xu and L. L. Yang, *Efficient computation of two-loop amplitudes for Higgs boson pair production*, *Phys. Rev. D* **104** (2021) L051901, [[2010.15649](#)].
- [54] J. M. Cornwall, D. N. Levin and G. Tiktopoulos, *Derivation of Gauge Invariance from High-Energy Unitarity Bounds on the s Matrix*, *Phys. Rev. D* **10** (1974) 1145.
- [55] B. W. Lee, C. Quigg and H. B. Thacker, *Weak Interactions at Very High-Energies: The Role of the Higgs Boson Mass*, *Phys. Rev. D* **16** (1977) 1519.
- [56] W. E. Caswell, *Asymptotic Behavior of Nonabelian Gauge Theories to Two Loop Order*, *Phys. Rev. Lett.* **33** (1974) 244.
- [57] D. R. T. Jones, *Two Loop Diagrams in Yang-Mills Theory*, *Nucl. Phys. B* **75** (1974) 531.
- [58] D. J. Broadhurst, N. Gray and K. Schilcher, *Gauge invariant on-shell $Z(2)$ in QED, QCD and the effective field theory of a static quark*, *Z. Phys. C* **52** (1991) 111–122.
- [59] M. Czakon, A. Mitov and S. Moch, *Heavy-quark production in gluon fusion at two loops in QCD*, *Nucl. Phys. B* **798** (2008) 210–250, [[0707.4139](#)].

- [60] M. Czakon, A. Mitov and S. Moch, *Heavy-quark production in massless quark scattering at two loops in QCD*, *Phys. Lett. B* **651** (2007) 147–159, [[0705.1975](#)].
- [61] K. Melnikov and T. van Ritbergen, *The Three loop on-shell renormalization of QCD and QED*, *Nucl. Phys. B* **591** (2000) 515–546, [[hep-ph/0005131](#)].